Coupled multiscale modeling and pathway analysis for prediction of drug efficacy in cystic kidney diseases

Sherry G Clendenon[1], Rita M de Almeida[2,3], Guilherme M Oliveira[1], Julio Belmonte[4], Robert L Bacallao[5], James A Glazier[1]

[1]Biocomplexity Institute and Department of Intelligent Systems Engineering, Indiana University, Bloomington, IN, 47405, USA;
[2]Biocomplexity Institute and Department of Physics, Indiana University, Bloomington, IN, 47405, USA;
[3]Instituto de Física and Instituto Nacional de Ciência e Tecnologia, Universidade Federal do Rio Grande do Sul, 91501-970, Porto Alegre, RS, Brazil; [4]EMBL Heidelberg, 69117 Heidelberg, Germany;
[5]Division of Nephrology, Department of Medicine, Richard Roudebush VAMC and Indiana University School of Medicine, Indianapolis, IN, 46202, USA.

Introduction

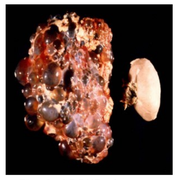

Fig. 1. ADPKD kidney (left). Normal (right).

Autosomal dominant polycystic kidney disease (ADPKD) is the most common genetic cause of kidney failure in the U.S, occurring in 1:700 to 1:1000 individuals with disease penetrance of 100%. ADPKD is characterized by progressive accumulation and growth of epithelial kidney cysts (Fig. 1) and results in kidney failure by the fifth or sixth decade of life. Currently there is no FDA approved treatment for ADPKD and the only therapeutic options for patients are dialysis or renal transplantation (Bolignano 2015; Boucher and Sandford, 2004). The genes responsible for ADPKD, Polycystin-1 and Polycystin-2 (PC1 and PC2) were identified in the1990s and a period of intense study ensued (Cai 1999; Consortium, 1995; Consortium, 1994; Hughes 1995; Mochizuki 1996). PC1 was found to localize to cilia, adherens junctions and focal adhesions and PC2 to cilia and to the endoplasmic reticulum (Chapin and Caplan, 2010). Mutations in either PC results in defective cilia mediated signaling (Avner and Sweeney, 2006). Downstream signaling pathways affected include; calcium, mTOR, p21/Waf, Ras/B-Raf/ERk and STAT signaling and cAMP stimulated growth (Boucher and Sandford, 2004; Wilson, 2004). Drugs that perturb many of these known pathways have had promising experimental results, but to date, none have succeeded in translating from bench to bed-side. Suppression of cyst emergence and growth will certainly involve some or all of these known pathways, but a need remains to identify an effective therapeutic approach. Cyst formation has been clearly demonstrated in PC knockout and knock-in animal models, yet it is still unknown exactly how PC mutations can cause the focal changes in epithelial organization that lead to cyst formation. We do know that multiple cell-cell adhesion changes accompany cyst formation in ADPKD (Blaschke et al., 2002; Charron et al., 2000; Huan and van Adelsberg, 1999; Roitbak et al., 2004) and our group's recent paired computational and experimental work further supports the role of dysregulated adhesion in ADPKD by showing that decreased cell-cell adhesion is necessary and sufficient to initiate cyst formation (Figs. 3-8, and Belmonte et. al. 2016).

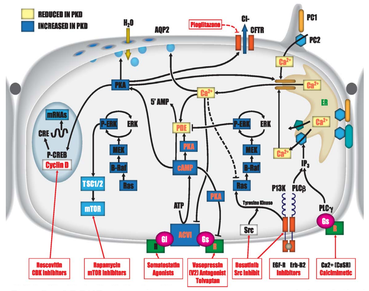

Fig. 2. ADPKD signaling pathways targeted by failed drug trials. Modified from Gattone & Bacallao, J Genet Synd Gene Therapy 2011.

We used genome wide expression screening to identify new signaling pathways changed in ADPKD.

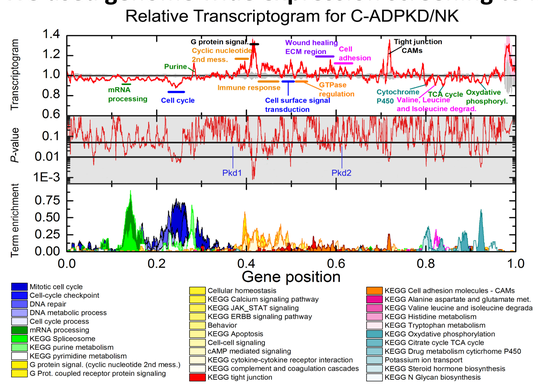

Fig 9. G-protein signaling is highly enriched in ADPKD tissue. Transcriptograms give an integrated visualization of genome wide gene expression data by projecting expression levels onto a functionally ordered gene list producing a genome wide expression profile (Rybarczyk-Filho 2011, da Silva 2014, Szklarczyk 2015).The **x**-axis indicates the relative position in the ordered list of 9684 genes. Upper panel: We present the relative transcriptograms as means ± s.e.m. with C-ADPKD (red line ± pink region) and NK (black line ± gray region) given relative to NK. Center panel (shaded gray): **P**-value from a two tailed Weyl's t-test for each point of the transcriptogram. Horizontal lines mark **P** = 0.05 and **P** = 0.01. We label the location in the ordered list of Pkd1 and Pkd2, the causative genes for ADPKD. Lower panel: Term enrichment for transcriptogram regions with gene expression significantly different from normal. A term enrichment value of 1 on the y-axis indicates that all genes in an interval of radius r=30 participate in a given GO term or KEGG pathway. Peaks mark regions enriched with genes related to the term or pathway indicated in the legend. The legend orders the terms/pathways from left to right. The most highly enriched region in the comparison of C-ADPKD/NK is in G-protein signaling. The most highly enriched gene sets within this region are phosphodiesterases (PDEs), specifically PDE's 5, 6 and 9 (de Almeida 2016) that regulate cGMP levels and activate signaling through PKGs.

We linked pathways changed in ADPKD to cell behavior drivers of cyst initiation using pathway analysis, then built a network diagram and corresponding SBML subcellular model, for inclusion in the VT model.

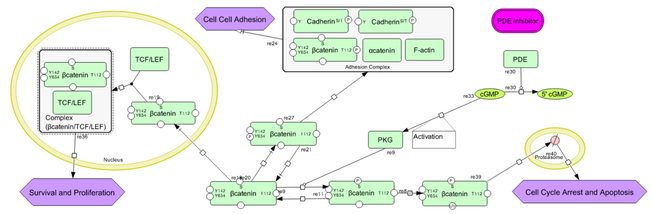

Fig. 10. PDE inhibition induces sustained levels of intracellular cGMP, activates downstream PKG, resulting in the inhibition of proliferation, induction of apoptosis, and changes in cell-cell adhesion (cadherin expression). We hypothesize that this is the mechanism by which sildenafil reduces cyst growth in vitro and in vivo (in mice). We used CellDesigner software (celldesigner.org, Funahashi 2003, Funahashi 2008) to build network diagrams and the corresponding SBML models for PDE inhibition and its linkage to downstream effects on cell-cell adhesion, cell death and cell proliferation. This network will be linked with CompuCell3D (CC3D) through Systems Biology Workbench (SBW) for simulation and parameter scanning. The complete VT model will use CC3D as a "marshaling point" with CC3D as an integrator that runs the VT model, time steps the subcellular reaction networks in SBML (Andasari 2012) (and future whole body PBPK/SBML models), and transfers values between scales.

Our VT model predicted and experiments confirmed roles for cell adhesion and proliferation in cyst initiation.

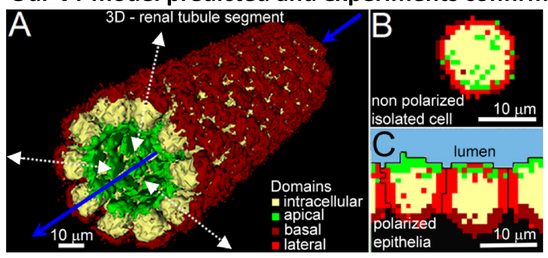

Fig. 3. Renal tubule segment and renal epithelial cell models. (a-c) Epithelial cells have 4 compartments representing basal (dark red), apical (green), lateral (red) and cytoplasmic (yellow) regions. Transparent black represents extracellular matrix (ECM). Light blue represents lumen in (c). (a) 3D renal tubule segment model. Dashed white arrows represent transport across epithelial layer and solid blue arrows represent fluid flow through tubule lumen. Lateral (red) compartments and lumenal fluid are not shown in the 3D tubule rendering. (b) Without cell-substrate or cell-cell binding cues, surface compartments representing adhesion molecules randomly distribute near the cell surface. (c) When renal epithelial cells contact other cells, lumen or ECM the cell surface domains arrange themselves according to their adhesive affinities creating ordered apical, basal and lateral domains.

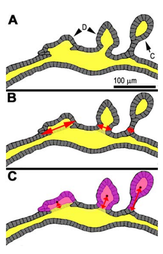

Fig. 4. Tracings of images of isolated human nephrons from Baert et al. we quantified cyst morphology as the ratio of cyst height (C) to cyst neck (B) diameter. (A) shows morphologies of two saccular dilations (arrow-heads labeled D) and a simple cyst (arrow labeled C).

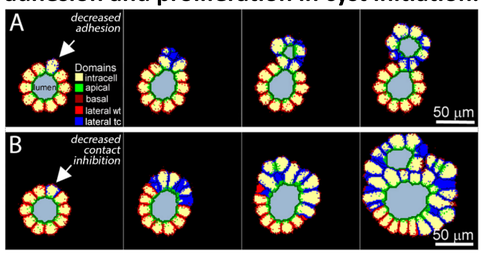

Fig. 5. Changes in adhesion and proliferation produce distinct ranges of cyst morphology. 2D transverse slice views of 3D simulations. (a) Reduced wild-type cell to target cell (WT-TC) adhesion results in loss of contact inhibition and increased proliferation of TCs to form a cyst that grows out of the WT tubule and connects to the tubule via a narrow neck where TC and WT cells touch. (b) Increased proliferation due to decreased contact inhibition (increased αc) inTCs while holding WT-TC adhesion constant, results in lateral spread of TCs within the surface of the tubule, followed by formation of cysts that remain spread across and closely apposed to the surface of the tubule. We apply the same metric as was used for the human cysts, ratio of cyst height to cyst neck to quantify simulation results.

We examined two hypothetical cell-level mechanisms by which abnormal expression of cadherin-8 could initiate cyst formation: i) reduction of cell-cell adhesion, which then leads to changes in proliferation or ii) direct reduction of contact inhibition of proliferation with no change in cell-cell adhesion. To test these mechanisms we built a 3D virtual-tissue (VT) computer model of the renal tubule using the CompuCell3D (CC3D) modeling environment (Swat et al., 2012). Our VT simulations predicted that either mechanism could initiate cyst formation, however only loss of adhesion simulations produced morphologies matching in vitro cadherin- 8 induced cysts (Belmonte et al., 2016).

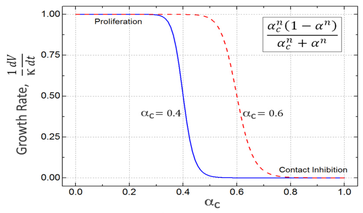

Fig. 6. Dependence of growth rate on fractional area of cell-cell contact, α. Values of $\alpha > \alpha_c$ contact-inhibit cell growth. Blue and red lines show the dependence of cell growth rate on α for α_c= 0.4and 0.6, respectively.

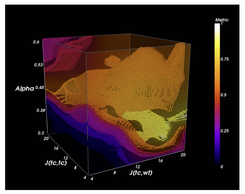

Fig. 7. 3D isosurface of cyst initiation morphology parameter space. Color in-dicates morphology metric of cyst height over cyst neck diameter. Black regions reflect baseline parameters where cyst formation does not occur. Yellow-white regions produced stalk type cysts.

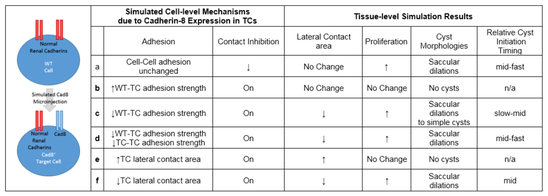

	Simulated Cell-level Mechanisms due to Cadherin-8 Expression in TCs		Tissue-level Simulation Results			
	Adhesion	Contact Inhibition	Lateral Contact area	Proliferation	Cyst Morphologies	Relative Cyst Initiation Timing
a	Cell-Cell adhesion unchanged	↓	No Change	↑	Saccular dilations	mid-fast
b	↑WT-TC adhesion strength	On	No Change	No Change	No cysts	n/a
c	↓WT-TC adhesion strength	On	↓	↑	Saccular dilations to simple cysts	slow-mid
d	↓WT-TC adhesion strength ↓TC-TC adhesion strength	On	↓	↑	Saccular dilations	mid-fast
e	↑TC lateral contact area	On	↑	No Change	No cysts	n/a
f	↓TC lateral contact area	On	↓	↑	Saccular dilations	mid

Fig. 8. Simulated cell-level effects of Cad-8 expression on tissue-level outcomes. In wild type (WT) simulated cells, contact between cells is sufficient to inhibit proliferation. Potential cell-level modes of action of cad-8 knock-in TCs include: a) Disruption of contact-inhibition of proliferation with no change in adhesion; b) Increased adhesion between WT and TC cells; (c) Reduced adhesion between WT and TCs; d) Reduced adhesion between both WT-TC and TC-TC; e) Increased TC lateral contact area; (f) Reduced TC lateral contact area. Each produces distinct combinations of cyst morphologies and timings of initiation.

Concurrently we tested pathway inhibitors on in vitro and in vivo cyst formation experimental models.

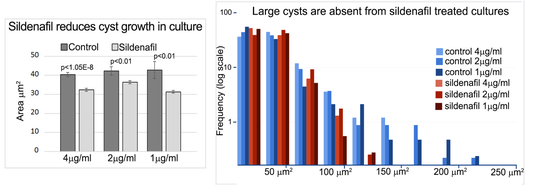

Fig. 11. Sildenafil treatment is effective in reducing growth of cysts from tubules in 3D culture. A. Using our human kidney cell cystogenesis assay we tested whether the prototypical PDE inhibitor, sildenafil (Viagra) would prevent or reduce cyst formation. Average cyst area was significantly reduced in Viagra treated cultures. No dose response was seen, indicating that a lower dosage is likely to be similarly effective. Lower dosages will be tested. Frequency distribution analysis shows that average cyst size is reduced because large cysts are absent from Viagra treated cultures. This complete absence of large cysts has greater potential to slow the progression of polycystic kidney diseases than a simple small reduction in all sizes of cysts. One way Anova analysis F-value = 11.65, HSD (alpha=0.05) 8.49, HSD (alpha=0.01) 10.10, C 4mg/ml vs S4mg/ml p<0.05, C 2mg/ml vs S 2mg/ml p<0.01, C 1mg/ml vs S 1mg/ml p<0.01

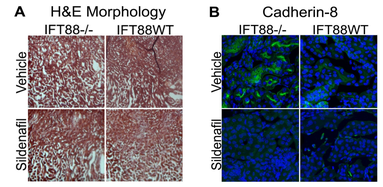

Fig. 12. Sildenafil treatment abrogates cystic phenotype and aberrant cadherin-8 expression in IFT88-/- mice. Using the IFT88 mouse model of PKD, tamoxifen was injected on P7, vehicle or drug treatment was started on P14 and kidneys were harvested on P40. A. Top half of each image is medulla and bottom half of each image is cortex. Preliminary data shows that sildenafil treatment lessens the cystic phenotype in the cortex of IFT88-/- mice. B. Kidney sections were labeled with antibody that labels cadherin-8 (green) and DAPI to label nuclei (blue). Confocal images show that cadherin-8, a cell-cell adhesion protein normally only expressed in early embryogenesis, in ADPKD kidneys or some kidney cancers, is expressed in IFT88-/- mouse kidneys. Sildenafil treatment reduces cadherin-8 expression in IFT88-/- kidneys. Upregulation of cadherin-8 (a weakly adhering cadherin) results in decreased cell-cell adhesion and cyst formation in vitro, and is seen in human ADPKD cysts.

Conclusion

We have developed a practical and efficient approach using VT modeling for prediction of drug efficacy in inhibition of kidney cyst formation.
1) Define cell behaviors that drive tissue pathogenesis through paired Virtual Tissue simulations and biological experiments.
2) Identify signaling pathways that drive abnormal cell behaviors and link them into the VT model.
3) Identify existing drugs for reuse that affect these pathways.
4) (In progress) Run VT simulations to predict drug efficacy (and off target effects), followed by biological testing of drugs prioritized by simulation.
We anticipate that this approach can be applied to other abnormal biological processes.

Bolignano et al., 2015. *Cochrane Database Syst Rev.* 7:CD010294
Boucher and Sandford, 2004. *European J Human Gen*. 12:347-354.
Cai et al., 1999. *J Biol Chem*. 274:28557-28565.
Consortium, 1995. *Cell.* 81:289-298.
Consortium, 1994. *Cell.* 78:725.
Hughes et al., 1995. *Nat Gen.* 10:151-160.
Mochizuki et al., 1996. *Science*. 272:1339-1342.
Chapin and Caplan, 2010. *J Cell Biol.* 191:701-710.
Avner and Sweeney, 2006. *Cell and tissue res* 326.3 (2006): 671-685.
Wilson, 2004. *Int J Biochem Cell Biol*. 36:1868-1873.
Blaschke et al., 2002. *Int J Cancer.* 101:327-334.
Charron et al., 2000. *J Cell Biol.* 149:111-124.
Huan and van Adelsberg, 1999. *J Clin Invest.* 104:1459-1468.
Roitbak et al., 2004. *Mol Biol Cell.* 15:1334-1346.
Belmonte et. al. 2016. *Mol Biol Cell* 27.22 (2016): 3673-3685.
Swat et al., 2012. *Methods Cell Biol.* 110, 325-366.
Rybarczyk-Filho 2011. *Nucleic Acids Res*, *39*(8), 3005–3016.
da Silva 2014. *BMC Genomics*. 2014.
Szklarczyk 2015. *Nucleic Acids Res*. 2015;43:D447-52.
de Almeida 2016. *Hum Gen* 10.1 (2016): 37.
Funahashi 2003. *BIOSILICO*, 1:159-162.
Funahashi 2008. *Proc. IEEE* 96:81254 - 1265.
Andasari 2012. *PloS one*. 7(3):e33726.

Poster #1:37 IMAG/MSM 10th Anniversary Meeting, Bethesda MD, March 2017